

INVESTIGATION OF THE EFFECT OF LEAD ION (Pb^{2+}) CONCENTRATION ON THE OPTICAL AND SOLID STATE PROPERTIES OF CHEMICALLY DEPOSITED $\text{Mn}_3\text{O}_4/\text{Pb}_{1-x}\text{S}$ HETEROJUNCTION THIN FILMS

C. AUGUSTINE^{a,b*}, M. N. NNABUCHI^b, P. E. AGBO^b,
F. N. C. ANYAEGBUNAM^a, R. A. CHIKWENZE^a, C. N. NWOSU^a,
P. N. KALU^a, U. UBA^a, R. O. OKORO^c, S. O. ONYISHI^d

^a*Department of Physics/Geology/Geophysics, Alex Ekwueme Federal University Ndufu-Alike Ikwo, Ebonyi State, Nigeria*

^b*Department of Industrial Physics, Ebonyi State University, Abakaliki, Ebonyi State, Nigeria*

^c*Department of Physics, Ebonyi State College of Education, Ikwo, Ebonyi State, Nigeria*

^d*Department of Physics, Federal College of Education, Eha-amufu, Enugu State, Nigeria*

The studies of the semiconductor core-shell nanoparticles have advanced at a rapid pace because of the fact that their optical properties can be systematically tuned by varying their sizes. This article studies the effects of Pb^{2+} concentration ($x = 0.9, 0.8$ and 0.7) on the optical and solid state properties of $\text{Mn}_3\text{O}_4/\text{Pb}_{1-x}\text{S}$ core-shell thin films. The elemental components of Mn, Pb, S and O were quantitatively obtained from RBS analysis. The optical properties were investigated from spectroscopy measurements of absorbance. Experiments showed that the growth parameter greatly influence the optical and solid state properties of $\text{Mn}_3\text{O}_4/\text{Pb}_{1-x}\text{S}$ thin films. The optical absorption characteristics of $\text{Mn}_3\text{O}_4/\text{Pb}_{1-x}\text{S}$ thin films suggest that it could be coated on solar collectors for enhanced solar energy collection. The direct, indirect band gaps and Urbach energy varied with concentration exhibiting a decreasing trend. The direct band gap varied from 4.10eV for 0.1M, 4.00eV for 0.2M and 3.90eV for 0.3M. The indirect band gap varied from 3.70eV for 0.1M, 3.60eV for 0.2M and 3.45eV for 0.3M. The Urbach energy varied from 3.75eV for 0.1M, 3.65eV for 0.2M and 3.60eV for 0.3M. The values of all the optical and solid state properties investigated vary directly with concentration except transmittance which is the reverse. Thus, the optical and solid state properties of $\text{Mn}_3\text{O}_4/\text{Pb}_{1-x}\text{S}$ thin films deposited by the chemical bath method can be tuned by deliberately controlling the concentration of the precursors for various optoelectronic applications including its application as absorber layer in solar cells. The large band gap possessed by $\text{Mn}_3\text{O}_4/\text{Pb}_{1-x}\text{S}$ thin films suggest that the films can be used for applications where high voltage, frequencies and temperature are required such as light-emitting diodes, transducers, RF radio processing and power switching applications.

(Received May 7, 2018; Accepted September 17, 2018)

Keywords: Concentration, band gap, solar, optical, solid state

1. Introduction

The growth of thin films using highly technological, advanced and very expensive techniques for optical, electronic and optoelectronic device application has become an industry in most developed countries. However, in third world countries, these advanced techniques have not been widely utilized because of their complexity and the poverty of the third world countries. Hence, the growing interest in developing simple and cheap techniques of depositing thin films. The chemical bath deposition technique offers the simplest, cheapest, most economical and affordable method of depositing thin films of various kinds.

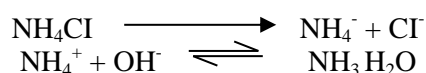
* Corresponding author: emmyaustine2003@yahoo.com

The chemical bath deposition technique has found wide acceptance among researchers in the field of thin films. Among the pioneers in the use of this method is Cashatan (1946) [1] who used the technique to prepare PbS thin films for infrared applications. Roberts and Baines (1958) [2] prepared PbSe using this technique. This was followed by the work of Bode (1966) [3]. For large area deposition and scale application, this technique gained prominence only in the late 70's and 80's through the works [4-10]. Recently, this technique was extended to the deposition of core-shell thin films of TiO₂/Fe₂O₃ [11], TiO₂/ZnO [12], TiO₂/CuO [13], TiO₂/NiO [14], ZnO/ZnS [15], PbS/CdS [16] among others. In our previous research works, we used this technique to deposit PbS/NiO, PbS/CdO, PbS/NiO/CdO and Mn₃O₄/PbS heterojunction thin films [17-20].

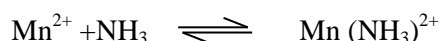
The use of heterojunction (HJ) with large band gap window material and a small band gap absorber material is a means to reduce the surface recombination loss that might otherwise dominate in direct band gap materials [12]. The formation of Mn₃O₄/Pb_{1-x}S thin films expands the semiconductor material possibilities for solar photovoltaic, high temperature and high frequency applications. We had investigated the effect of thermal annealing on the optical and solid state properties of Mn₃O₄/PbS thin films in our previous work [20]. In this present work, we report on the effect of Pb²⁺ concentration on the optical and solid state properties of Mn₃O₄/Pb_{1-x}S heterojunction thin films grown by chemical bath deposition technique.

2. Experimental

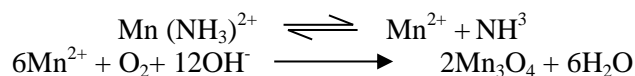
Chemical bath deposition technique was used to deposit the films on plane glass substrates. Before deposition, the substrates were degreased by hydrochloric acid treatment, rinsed with distilled water and left to dry in dust-free environment. All reagents were of analytical grade and used without further purification. 1M manganese (II) chloride tetrahydrate (MnCl₂·4H₂O) was weighed exactly and dissolved in distilled water. With the solution being continuously stirred, the MnCl₂ aqueous solution was mixed with an appropriate amount of 1M ammonium chloride NH₄Cl. The pH value of the solution was adjusted with ammonia NH₃·H₂O to 10.0. After stirring, this clear and homogeneous aqueous solution was used as the precursor solution for Mn₃O₄ thin film. The pre-treated substrates were floated on the surface of the solutions to prevent particles formed in the solution from accumulating on the substrate surface. The beakers containing the precursor solution were maintained at desired temperature for different deposition duration in order to obtain the proposed films. To deposit Mn₃O₄/Pb_{1-x}S core-shell thin films, the substrates coated with Mn₃O₄ deposits were dipped in an aqueous solution, consisting of lead (II) nitrate [Pb (NO₃)₂ (x = 0.7M-0.9M)], 1M thiourea [SC (NH₂)₂], 1M sodium hydroxide (NaOH 1M). The composition of the core was diluted with 24mls of distilled water and heated for 5hours while that of the shell was diluted with 35mls of distilled water at room temperature. The substrates were dipped vertically into the center of the reaction baths in such a way that they did not touch the bottom or walls of the bath containers. Several variations of the bath constitutions of each compound whose films were to be deposited was employed. For a chosen standard reaction bath for such a compound the substrates was allowed to stay in the bath for different dip times. This is to allow the growth condition to be optimized and the baths standardized. After deposition, the films were washed in distilled water and drip dried in air after which two of them was annealed at different temperature while one was left un-annealed to serve as the control. The possible chemical reaction for the formation of Mn₃O₄ thin films proceeded as follows [21]:



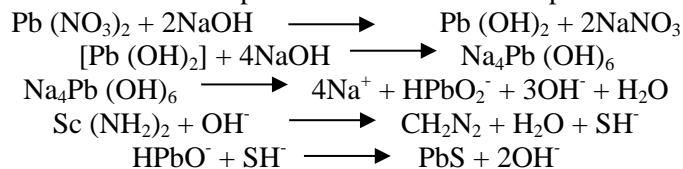
Mn²⁺ cations form ammine complexes of Mn (NH₃)²⁺ with NH₃ (aq) in moderately basic media as:



The solution is acidic at this point with P^H of 5.9. Ammonia solution was dropped to the solution to adjust P^H up to 10.0 and the solution became alkaline. Due to the alkalinity, the $Mn(NH_3)^{2+}$ was unstable leading to the following reactions:



The chemical reaction for the deposition of PbS thin films proceeded as follows [22]:



When lead nitrate was dissolved in distilled water, it releases Pb^{2+} ions. With the addition of sodium solution, white cloudy precipitate appeared but decreased with time and eventually became smaller than the original precipitate. With the addition of thiourea solution into the bath there was noticeable physical change. When finally distilled water was added, the precipitate remained while a whitish liquid formed at the top of the precipitate. After sometime the precipitate was black followed by a silvery colour with dark brown colours on top. The rings remained the same as well as the bulk of the liquid.

Optical absorption data were obtained with a thermo scientific GENESYS 10S model UV-VIS spectrophotometer at normal incidence of light in the wavelength range of 300-1000 nm. Rutherford backscattering (RBS) was used to determine the elemental composition, depth profile and thickness of the films by Proton Induced X-ray Emission (PIXE) scans on the samples from a Tandem Accelerator Model 55DH 1.7MV Pellaton. The structural analysis was done with Rigaku Ultima IV X-ray diffractometer equipped with a graphite-monochromated CuK_{α} radiation source (40KV, 30mA) of $\lambda = 0.15406nm$.

3. Results and discussion

The elemental components of Mn, Pb, S and O were quantitatively obtained from RBS analysis as shown in the micrograph (Fig.1). Other elements present could have come from the glass substrate and some impurities.

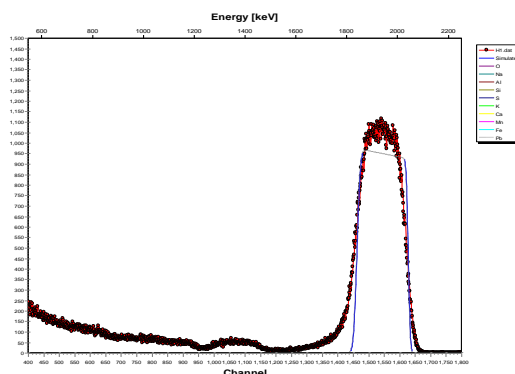


Fig. 1. RBS micrograph of a sample of $Mn_3O_4/Pb_{1-x}S$ thin film.

The optical absorption were taken in the range of wavelengths 300 – 1000 nm. The graph of absorbance against wavelength is shown in Fig. 2. The representatives of optical absorbance reveals that the absorbance of the film increases with increase in molarity of Pb^{2+} concentration.

The absorbance is generally higher in the UV region compared to other regions. From Fig. 2, it is observed that the absorbance of the three samples decreased with increasing wavelength except for 0.1M layer which depicts fairly constant absorbance in the wavelength range (350nm-1000nm). The peak absorbance are 1.25 (a.u), 3.90(a.u) and 4.00(a.u) for 0.1M, 0.2M and 0.3M respectively. Generally, the absorbance, A , vary in the following range $0.35 \leq A \leq 1.25$, $0.50 \leq A \leq 3.90$, and $1.25 \leq A \leq 4.00$ for 0.1M, 0.2M and 0.3M samples respectively. High absorbance in the UV region as depicted by $Mn_3O_4/Pb_{1-x}S$ thin films placed them as useful materials in the formation of p-n junction solar cells with other suitable materials for photovoltaic applications [29]. The absorption edge of the three samples occurred around 340 nm. As observed in the transmittance spectra (Fig.3), the transmittance vary in opposite manner, decreasing with concentration exhibiting a minimum for 0.3M film sample. The graph shows that the samples under study exhibit higher transmittances at longer wavelengths (NIR region). The highest transmittance was observed for the 0.1M layer, while the lowest value of transmittance was recorded by the 0.3M layer. The transmittance generally vary from 5% to 50% for 0.1M sample, 0.1% to 36% for 0.2M sample and 0.1% to 7.5% for 0.3M sample. Accordingly, red-shifting is observed in the transmittance curve and this could be attributed to increased particle dimension in different matrix indicating the incorporation of PbS - shell into the core - Mn_3O_4 binary component. The concentration effect on the optical transmittance of thin films has been reported by other research group [30-32]. The transmittance characteristics of $Mn_3O_4/Pb_{1-x}S$ thin films suggest that the films may be used as good materials for thermal control coatings inside buildings. The IR region is that region of the electromagnetic spectrum that is responsible for heating up the environment, thus for the purpose of heating up the interior of a building, materials with high transmittance in the infrared region are required. $Mn_3O_4/Pb_{1-x}S$ thin films exhibited relatively high transmittance in the NIR region and may be used as spectrally selective window coatings in cold climate to facilitate transmission of ViS and NIR while suppressing the UV portion of the solar radiation. The property of relatively high transmittance in the NIR exhibited by the 0.1M layer placed it as a good material for construction of poultry roofs and walls to admit infrared radiation into the building for warming young chicks. This will substantially reduce the cost of energy consumption incurred from the use of electric bulbs, stoves and electric lambs. These findings are in agreement with that of Augustine and Nnabuchi (2018) for CuO/PbS thin films [33].

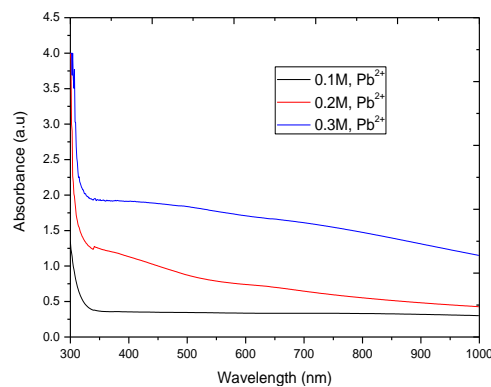


Fig. 2. Plot of absorbance against wavelength at different concentrations.

The reflectance of the film samples was calculated using the relation [34]

$$R = 1 - [T \exp(A)]^2 \quad (1)$$

Where R is the reflectance, T is transmittance and A is the absorbance. The plots of reflectance as a function of wavelength is shown in Fig. 4. Generally, the film samples displayed low values of reflectance exhibiting a minimum for 0.3M sample. The low values of reflectance is an indication

that most of the light were either absorbed or transmitted by the films. The reflectance spectra shows that 0.1M sample was almost constant immediately after the absorption edge in the wavelength range 350-900 nm.

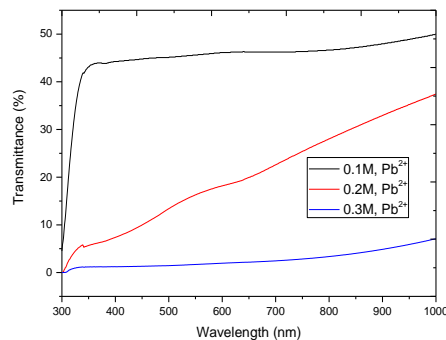


Fig. 3. Plot of transmittance against wavelength at different concentrations.

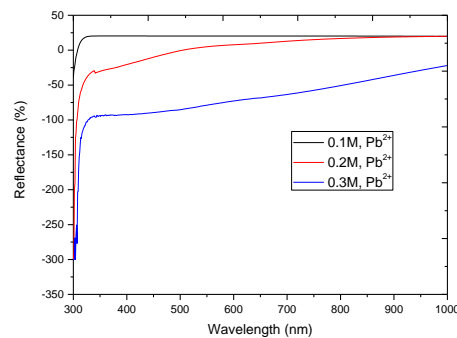


Fig. 4. Plots of reflectance as a function of wavelength at different concentration.

The absorption coefficient α , associated with the strong absorption region of the films, was computed from transmittance (T) and the film thickness (t) using equation (2) [35].

$$\alpha = \frac{1}{t} \ln \left[\frac{100}{T\%} \right] \quad (2)$$

Fig.5 shows the plots of the absorption coefficient (α) against photon energy ($h\nu$) at different concentration. The optical absorption coefficient increases with increasing photon energy (decreasing wavelength). The absorption coefficient of the 0.2M layer is higher compared to other layers. α generally vary from 7.5×10^2 to $2.75 \times 10^3 \text{ m}^{-1}$, 1×10^3 to $8.5 \times 10^3 \text{ m}^{-1}$ and 1.75×10^3 to $6.0 \times 10^3 \text{ m}^{-1}$ for 0.1M, 0.2M and 0.3M samples respectively. The range of the optical absorption coefficient is an indication that the films may be utilized in different optoelectronic devices.

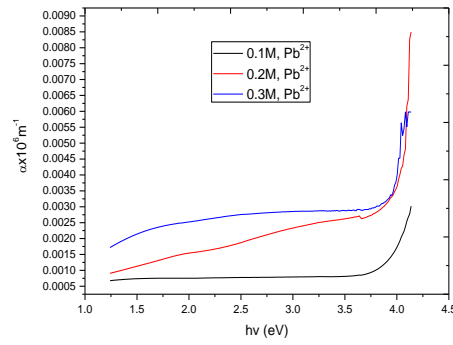


Fig. 5. Absorption coefficient against photon energy plots of $Mn_3O_4/Pb_{1-x}S$ at different molarities.

Based on the obtained optical absorption measurements, the square of absorption coefficient $(\alpha hv)^2$ was plotted as a function of photon energy (hv). Such plot is shown in Fig.6. A steep optical absorption feature is obtained, indicating good homogeneity in the shape and size of the grains as well as low defect density near the band edge. As can be seen, $(\alpha hv)^2$ vary almost linearly with hv above the band gap energy (E_g). Accordingly, the following equation for a direct inter-band transition can be applied [36].

$$\alpha hv = A(hv - E_g)^n \quad (3)$$

where α is the optical absorption coefficient, A is an energy independent constant but depend on the refractive index and the effective masses of the hole and electron respectively [36], E_g is the energy band gap, and n is an index that characterises the nature of the transition. For $n = 1/2$, the transition is generally accepted to be direct. For $n=2$, the transition is indirect. The plots of $(\alpha hv)^{1/2}$ as a function of photon energy was done to determine the indirect band gap of the samples. Such plots are depicted in Fig. 7.

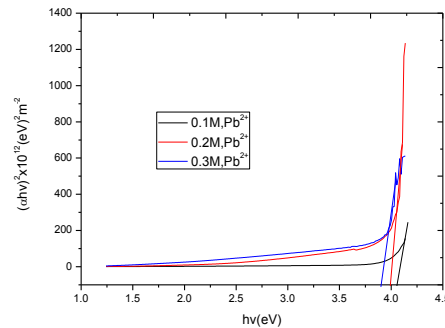


Fig. 6. Plots of $(\alpha hv)^2$ as a function of hv at different molar concentration.

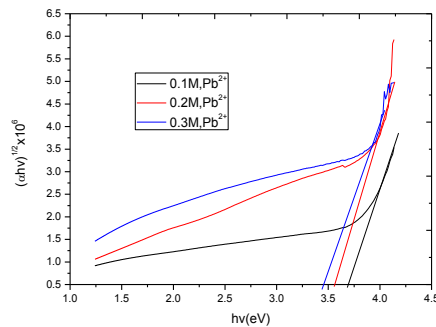


Fig. 7. Plots of $(\alpha hv)^{1/2}$ as a function of hv at different molar concentration.

The direct optical band gap energy deduced by extrapolating the straight line portion to the energy axis at $(\alpha hv)^2 = 0$ are obtained to be 4.10eV, 4.00eV and 3.90eV for 0.1M, 0.2M and 0.3M samples respectively. The indirect band gap are 3.70eV for 0.1M, 3.60eV for 0.2M and 3.45eV for 0.3M. The direct and indirect band gaps at different molarity are tabulated in table 1. The absorption edge shifted to longer wavelength indicating decrease in band gap. The shifting of E_g to lower values is a clear indication of band gap narrowing induced by increase in concentration of precursor solution. This behaviour is attributed to the increase in grain size and/or related phenomena, caused by the concentration effects. The successive decrease as shown in Figs. 6 and 7, clearly depicts the classic ‘‘Moss-Burnstein shifts’’. The wide band gap expands the possibility of using the films as window layers for solar cell fabrication.

In the case of the Urbach behaviour of the absorption edge, the spectral dependence of absorption coefficient (α) is described as [37, 38].

$$\alpha = \alpha_o \exp\left(\frac{hv}{E_u}\right) \quad (4)$$

According, equation (4) can be transform to equation of a straight line by taking the natural logarithm of both sides as:

$$\ln \alpha = \ln \alpha_o + \left(\frac{hv}{E_u}\right) \quad (5)$$

where α_o is a constant which denotes the point of convergence of the Urbach bundle, hv is the photon energy, E_u is the Urbach energy which characterizes the degree of the absorption edge smearing due to the crystalline lattice disordering caused by structural peculiarities as well as induced by external factors [39]. The graph of $\ln(\alpha)$ against hv was plotted to determine the Urbach energy (Fig.8). The tangent of the line around the absorption edge curve to $\ln(\alpha) = 0$ gives the Urbach energy as 3.75eV, 3.65eV and 3.60eV for 0.1M, 0.2M and 0.3M respectively. A strong correlation exist amongst the direct, indirect band gap and Urbach energy as indicated in the close range of values (Table 1). The Urbach energy decreases with concentration exhibiting minimum for 0.3M sample. The possible explanation of this behaviour is that the higher concentration i.e increase in thickness results in better crystallization of the films and hence more order and smaller density of localized states [40].

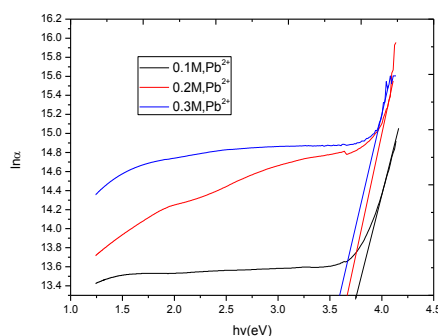


Fig. 8. Plots of $\ln(\alpha)$ as a function of hv at different molar concentration.

Table 1. The estimated values of band gap and Urbach energy at different molar concentration.

Concentration (M)	Direct band gap	Indirect band gap	Urbach energy
0.1	4.10	3.70	3.75
0.2	4.00	3.60	3.65
0.3	3.90	3.45	3.60

Fig. 9 shows the plots of the variation of the refractive index with photon energy ($h\nu$). The Refractive index, n is given in terms of the reflectance, R of the thin films that have $k^2 \ll n^2$ (where k is extinction coefficient) as [41]:

$$n = \frac{1+R}{1-R} + \sqrt{\frac{4R}{(1+R^2)} - k^2} \quad (6)$$

The results show a decreasing trend of the refractive index with decreasing wavelength (increasing photon energies). Such trend are commonly observed for most thin films of chalcogenides independent of the deposition technique [41]. However, the index of refraction of 0.3M layer was constant across the entire wavelength region. This could be as a result of the complex introduced by the negative reflectance values of 0.3M layer vis-a-vis the high absorbance values. The 0.1M layer shows higher index of refraction compared to the other two layers exhibiting a maximum of 2.6. Fig. 10 shows the plots of extinction coefficient (k) with photon energy. The extinction coefficient was calculated using the formula;

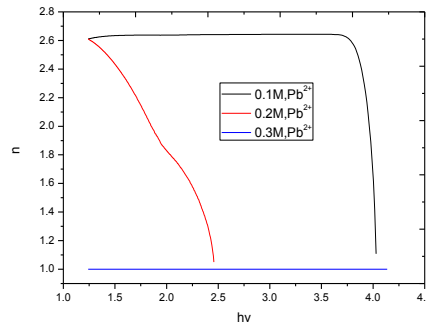


Fig. 9. Plots of refractive index (n) as a function of photon energy ($h\nu$) at different molar concentrations.

$$K = \frac{\alpha\lambda}{4\pi} \quad (7)$$

The extinction coefficient decreased up to the range of the photon energies at which the energy bandgaps occurred (region of the fundamental absorption) and then increased. However, the values of the 0.3M layer was higher in the visible and infrared regions compared to the extinction coefficient values of the other two layers.

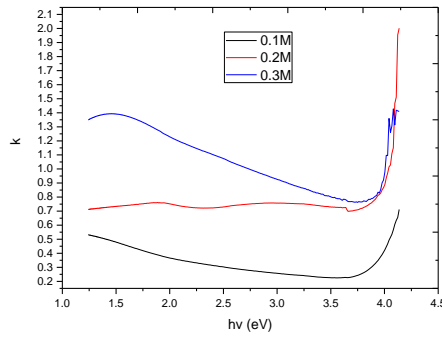


Fig. 10. Plots of extinction coefficient (k) vs $h\nu$ at different molar concentrations.

Fig. 11 shows the plots of the variation of the real part of the dielectric constant with photon energy ($h\nu$) while Fig. 12 gives that of the imaginary part of the dielectric constant with photon energy. A dielectric is actually an insulator (or poor conductor of electricity). This affects how light moves through materials. A high value of dielectric constant makes the distance inside the material looks longer so that the light travels slowly. It also ‘scrunches up’ the waves to behave as if the signal had a shorter wavelength. For use in capacitor, it must be high and for semiconductors, it must be low for high speed signal to take place. A dielectric may also be regarded as a continuous medium, which becomes polarized under the action of an electric field. The ratio of the polarization to the electric field producing it, being proportional to the electric susceptibility, χ_e is substantially independent of the field strength. The dielectric constant is then given by

$$K_\ell = 1 + \chi_\ell = \frac{\varepsilon}{\varepsilon_o} \quad (8)$$

where ε is the electric permittivity and ε_o is the permittivity of free space. In general, the dielectric constant is a complex quantity that is related to the complex refractive index by the equation [42, 43].

$$\varepsilon = \varepsilon_r + \varepsilon_i = (n - ik)^2 \quad (9)$$

where ε_r and ε_i are the real and imaginary parts respectively of dielectric and $(n - ik)$ is the complex refractive index. Hence,

$$\varepsilon_r = n^2 - k^2 \quad (10)$$

$$\varepsilon_i = 2ink \quad (11)$$

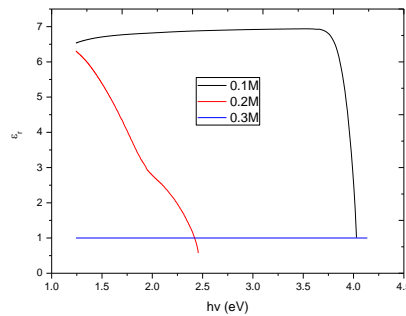


Fig. 11. Real dielectric constant (ε) as a function of photon energy ($h\nu$) at different concentrations.

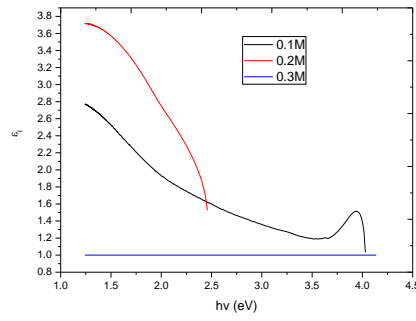


Fig. 12. Imaginary dielectric constant (ϵ_i) as a function of photon energy ($h\nu$) at different concentrations.

The physical implication of the dielectric constant is that electromagnetic waves incident on a vacuum can propagate through a sample when the real part is positive, but are totally reflected from the medium when it is negative. This constant is a characteristic property of a given dielectric material, which varies not only from one substance to another but also with the physical state of the material. The real and imaginary parts of the complex refractive index, which is defined for a substance that absorb as well as refract is given by [44],

$$n = \sqrt{\left(\frac{1}{2}\{\epsilon_r^2 + \epsilon_i^2\}^{\frac{1}{2}} + \frac{\epsilon_r}{2}\right)} \quad (12)$$

$$k = \sqrt{\left(\frac{1}{2}\{\epsilon_r^2 + \epsilon_i^2\}^{\frac{1}{2}} - \frac{\epsilon_r}{2}\right)} \quad (13)$$

When the frequencies are high, the semiconductor behaves like a perfect dielectric while at sufficiently low frequencies, both n and k are large and nearly equal (the conductivity is also high) and the semiconductor has a value of reflectance, which is nearly unity thereby becoming perfectly reflective.

As indicated in figure 11, the real part of the dielectric constant shows different behaviour for each sample. In 0.1M layer, the real part of dielectric increased with an increase in the photon energies up to a maximum 4.0eV and then decreases sharply. The 0.2M layer depicts a trend of decreasing values of real part of dielectric constant with increasing photo energies while the 0.3M layer was constant across the entire wavelength region and showed the least dependence of real dielectric with photo energy. It can also be seen that from the plots that the index of refraction (fig. 10) and real part of the dielectric constant behave alike. The plot of imaginary dielectric (ϵ_i) against photon energy ($h\nu$) shown in Fig. 12, depicts a pattern of decreasing values of the constant with increasing photon energy for all samples except 0.3M layer which is constant.

Fig. 13 shows the variation of the dielectric constant with the photon energy. The plots exhibited a trend of decreasing values of the dielectric constants with decrease in wavelengths (increasing photon energies) for 0.1M and 0.2M layers. The dielectric constant as shown in figure 13, for photon energies ≤ 4.0 eV, the values of the dielectric constants was between 2 to 10. These values are low enough for use of the layers for fabrication of devices with low capacitance requirements [45].

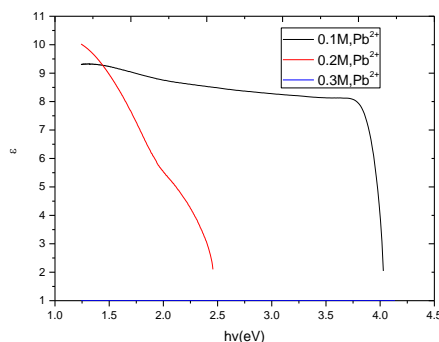


Fig. 13. Plots of dielectric constant (ϵ) as a function of photon energy at different concentrations.

4. Conclusions

$\text{Mn}_3\text{O}_4/\text{Pb}_{1-x}\text{S}$ core-shell thin films were successfully coated on the glass substrate by chemical bath deposition technique. The optical and solid state properties of the prepared films were analysed. The increase in the concentration of the precursor solution modified the optical and solid state properties of the deposited films. In particular, the band gap both direct and indirect of the films was red shifted with increase in concentration. The Urbach energy which indicated the level of defects in the films decreased with concentration exhibiting a minimum for 0.3M sample. The optical characteristics of the deposited films are found suitable in so many solar applications such as solar energy collection, photosynthetic coatings, anti-reflective coatings and fabricating optoelectronic devices. The large band gap possessed by $\text{Mn}_3\text{O}_4/\text{PbS}$ thin films suggest that the films can be used as window materials for solar cell fabrication as well high voltage power switching devices.

References

- [1] R. J. Cashatan, Journal of Optical Society of America, **136**, 356 (1946).
- [2] D. H. Robert, J. E. Baines, Journal of Physics and Chemistry Solids **6**, 184 (1958).
- [3] D. E. Bode, Physics of Thin Films **3**, Academic Press, New York, 123 (1966).
- [4] N. C. Sharma, D. K. Pandya, H. K. Sahgal, K. L. Chopra, Thin Solid Films **59** (2), 157 (1979).
- [5] R. C. Kainthla, D. K. Pandya, K. L. Chopra, Journal of Electrochemical Society **127**(2), 273 (1980).
- [6] I. Kaur, D. K. Pandya, K. L. Chopra, Journal of Electrochemical Society **127**, 943 (1980).
- [7] S. Bhattacharya, P. Pramanick, P. K. Basa, Thin Solid Films Lett. **149**, 181 (1987).
- [8] A. Cody, B. G. Books, B. Abeles, Solar Energy Materials **8**, 232 (1982).
- [9] P. K. Nair, M. T. S. Nair, Sol. Ener. Mater. **15**, 431 (1987).
- [10] G. B. Reddy, D. K. Pandya, K. I. Chopra, Sol. Ener. Mater. **15**, 153 (1987).
- [11] P. E. Agbo, M. N. Nnabuchi, D. U. Onah, Journal of Ovonic Research **7**(2), 29 (2011).
- [12] P. E. Agbo, M. N. Nnabuchi, Chalcogenide Letters **8**(4), 273 (2011).
- [13] P. E. Agbo, G. F. Ibeh, S. O. Okeke, J. E. Epke, Communications in Applied Sciences **1**(1), 38 (2013).
- [14] D. U. Onah, C. E. Okeke, E. I. Ugwu, J. E. Ekpe, An International Journal **3**(3), 62 (2015).
- [15] M. Kavitha, M. Saroja, V. K. Romesh, G. Jenifer, International Journal of Thin Films Science and Technology **5**(2), 137 (2016).
- [16] A. I. Onyia, M. N. Nnabuchi, Health and Environment, UNN, March 23-29 (2014)..
- [17] C. Augustine, M. N. Nnabuchi, F. N. C. Anyaegbunam, A. N. Nwachukwu, Digest Journal of Nanomaterials and Biostructures **12**(2), 523 (2017).
- [18] C. Augustine, M. N. Nnabuchi, F. N. C. Anyaegbunam, C. U. Uwa, Chalcogenide Letters **14**(8), 321.
- [19] C. Augustine, M. N. Nnabuchi, Journal of Ovonic Research **13**(4), 233 (2017).
- [20] M. N. Nnabuchi, C. Augustine, Materials Research Express, (2018).
- [21] Xu. Haiyan, Xu. Sile, W. Hao, Y. Hui, Journal of the Electrochemical Society **152**(2), 803 (2005).
- [22] S. Seghaier, N. Kamoun, R. Brini, A. B. Amara, Material Chemistry and Physics **97**, 71 (2006).
- [23] J. Li, Y. Xu, Y. Liu, D. Wu, Y. Sun, China. Particuology. **2**, 266 (2004).
- [24] M.A. Behnajady, N. Modirshahla, E. Ghazalian, Digest. J. Nanomater. Biostructure. **6**, 467 (2011).

- [25] V. Mote, Y. Purushotham, B. Dole, *J. Theor. Appl. Phys.* **6**, 1 (2012).
- [26] K. O. Ovid, *Rev. Adv. Mater. Sci.* **1**, 61 (2000).
- [27] N. Soltani, A. Dehzangi, A. Kharazmi, E. Salam, W. M. Yunus, B. Y. Majlis, M. R. Zare, E. Gharibshahi, N. Khalizadeh, *Chalcogenide Letters* **11**(2), 79 (2014).
- [28] G. Theophil Anand, L. John Kennedy, J. Judith Vijaya, *J. Alloy. Compd.* **581**, 558 (2013).
- [29] S. C. Ezeugwu, F. I. Ezeama, P. U. Asogwa, *Chalcogenide Letters* **7**(5), 369 (2010).
- [30] P. E. Agbo, P. A. Nwofe, L. O. Odo, *Chalcogenide Letters*, **14**(8), 357 (2017).
- [31] A. H. O. Al-khayatt, M. D. Jaafer, **6**(1), 27 (2014).
- [32] C. D. Lokhande, B. R. Sankapal, S. Mane, H. M. Pathan, M. Muller, M. Giersig, V. Ganesan, *Appl. Surf. Sci.* **193**, 1 (2002).
- [33] C. Augustine, M. N. Nnabuchi, *Materials Research Express*, **5**(3), 1-11 (2017).
- [34] P. E. Agbo, P. A. Nwofe, L. O. Odo, *Chalcogenide Letters* **14**(8), 357 (2017).
- [35] J. Bardeen, F. J. Blatt, L. H. Hall, (1954), *Proc. of Atlantic City Photoconductivity Conference*, J. Wiley and Chapman and Hall (1956).
- [36] V. Bilgin, S. Kose, F. Atay, I. Akyuz, *Mater. Chem. Phys.* **94**, 103 (2005).
- [37] Y. Natsume, H. Sakata, T. Hirayama, *Phys Stat Sol (A)* **148**, 485 (1995).
- [38] I. Studenyak, M. Kranjcec, M. Kurik, *International Journal of Optics and Applications* **4**(3), 76 (2014).
- [39] S. J. Ikhmayies, R. N. Ahmad-Bitar, *Journal of Materials Research and Technology* **2**(3), 221 (2013).
- [40] M. C. Tamargo, C. Hernandez, Ed., II – VI Semiconductor Materials and Their Application, Taylor and Francis, New York, 113-170 (2002).
- [41] B. Ismail, S. Mushtaq, A. Khan, *Chalcogenide Letters* **11**(1), 37 (2014).
- [42] B. G. Mahrov, A. Hgfeldt, L. Dloczuk, T. Dittrich, *Appl. Phys. Lett.* **84**(26), 5455 (2004).
- [43] F. Wooten, *Optical properties of solids*, Academic Press, New York (1972).
- [44] J. I. Pankove, *Optical processes in semiconductors*, Prentice-Hall, New York (1971).
- [45] P.A. Nwofe, P.E. Agbo, *Journal of Non-Oxide Glasses*, **9**(1), 9-17.